Lattice Boltzmann modeling of multicomponent diffusion in narrow channels

Seung Hyun Kim* and Heinz Pitsch
Department of Mechanical Engineering, Stanford University, California 94305-3035, USA

Iain D. Boyd
Department of Aerospace Engineering, University of Michigan, Michigan 48109-2140, USA

(Received 1 May 2008; revised manuscript received 8 December 2008; published 8 January 2009)

We investigate lattice Boltzmann (LB) modeling of multicomponent diffusion for finite Knudsen numbers. Analytic solutions for binary diffusion in narrow channels, where both molecular and Knudsen diffusion are of importance, are obtained for the standard and higher-order LB methods and validated against the results from the direct simulation Monte Carlo (DSMC) method. The LB methods are shown to reproduce the diffusion slip phenomena. In the DSMC method, while fluid particles are diffusely reflected on a wall, significant component slip and a kinetic boundary layer are observed. It is shown that a higher-order LB method accurately captures the characteristics observed in the DSMC method.

DOI: 10.1103/PhysRevE.79.016702 PACS number(s): 47.11.−j, 47.61.−k, 05.20.Dd

I. INTRODUCTION

Diffusion in nanoscale confined geometry is observed in both nature and engineering applications, e.g., catalysis and fuel cells. For the small Knudsen number (Kn) limit, where the characteristic length of the geometry is much larger than the mean free path of molecules, the diffusional flux is dominated by molecular collisions, and the constitutive relation between the flux and the concentration gradient is given by Fick's law [1] for binary mixtures away from a wall. For the large Kn limit, on the other hand, the flux is governed by collisions with walls, and the analytic solution for the mass flow rate is known for a simple geometry [2]. The focus of this paper is on multicomponent gaseous diffusion in the intermediate Kn regime, where both molecular and Knudsen diffusion are of importance.

For liquid-wall interactions of a binary mixture, Koplik and Banavar [3] showed that the individual species velocities vanish at a wall in their molecular dynamics (MD) simulations, which means the breakdown of Fick's law in the vicinity of a wall [4]. However, the thickness of the boundary layer where a conventional Fick's law breaks down was shown to be just about one diameter of liquid molecules, and Fick's law holds in most of the considered region [5]. In contrast to liquid, Mo and Rosenberger [6] found significant ″component slip″ for a gas mixture in their MD simulations and argued that the no-slip boundary condition for the small Kn limit results from the cancellation of the slip velocities for different components.

The slip phenomena in multicomponent mixtures have been extensively studied in the kinetic theory community [7–9]. Similar to slip velocity in the presence of velocity gradients, for multicomponent mixtures, concentration gradients parallel to a wall can also cause slip, the phenomena known as "diffusion slip." Diffusion slip phenomena were first discussed in Kramers and Kistemaker [10], where a formula for the diffusion slip velocity has been obtained using a simple kinematic argument, and several computational and theoretical studies for the diffusion slip have been performed after this pioneering work [7–9].

The lattice Boltzmann (LB) method [11–15] is a reduced-order kinetic model to reproduce hydrodynamics at the Navier-Stokes order or beyond. While the LB method is designed originally to mimic the Navier-Stokes hydrodynamics, significant progress in the modeling of single-component micro- and nanoscale flows has recently been made, especially for fluid-wall interaction models [16–21] and higher-order LB methods [22–24]. The slip velocity in multicomponent Couette flow has also been investigated for the standard LB method [25]. While one of the advantages of the LB method is the capability to model the physics of multicomponent and multiphase flows at a mesoscopic level [13,16], it remains an open question whether the LB method is able to capture the characteristics of multicomponent diffusion in the intermediate Kn regime and the diffusion slip.

In this paper, we investigate LB modeling of multicomponent diffusion for finite Knudsen numbers. In Sec. II, the LB equation for the binary mixture is presented. In Sec. III, analytic solutions for binary diffusion in narrow channels are obtained for the standard and higher-order LB methods. In Sec. IV, the analytic and numerical solutions for the LB methods are validated against reference solutions obtained using the direct simulation Monte Carlo (DSMC) method [26], and discussed with emphasis on the dependence of the diffusion flux on Kn, the diffusion slip, and the discrete lattice effects. The paper ends with the summary of the main conclusions.

II. LATTICE BOLTZMANN METHOD FOR MULTICOMPONENT MIXTURES

A. Discrete velocity BGK equation for multicomponent mixtures

Here, the kinetic equation for the binary mixture is based on the Bhatnagar-Gross-Krook (BGK) collision model [27]. The generalized model of Sirovich [28,29] can be written as

*shkcomb@stanford.edu

$$\partial_t f^\sigma + c_\alpha \partial_\alpha f^\sigma + g_\alpha^\sigma \partial_{c_\alpha} f^\sigma = J^{\sigma\sigma} + J^{\sigma\varsigma}, \tag{1}$$

where f^σ is the velocity distribution function of the species σ, c_α is the molecular velocity in the α direction, and g_α^σ is an acceleration. The self-collision term $J^{\sigma\sigma}$ and the cross-collision term $J^{\sigma\varsigma}$ are given by

$$J^{\sigma\sigma} = -\frac{1}{\tau_\sigma}(f^\sigma - f^{\sigma(0)}), \tag{2}$$

$$J^{\sigma\varsigma} = -\frac{1}{\tau_{\sigma\varsigma}}\frac{1}{c_\sigma^2}[(1-\beta)f^{\sigma(0)}(c_\alpha - u_\alpha^\sigma) + \beta f^{\sigma\varsigma(0)}(c_\alpha - u_\alpha)] \times (u_\alpha^\sigma - u_\alpha^\varsigma), \tag{3}$$

$$f^{\sigma(0)} = \frac{\rho_\sigma}{(2\pi c_\sigma^2)^{D/2}} \exp\left[-\frac{(c_\alpha - u_\alpha^\sigma)^2}{2c_\sigma^2}\right], \tag{4}$$

$$f^{\sigma\varsigma(0)} = \frac{\rho_\sigma}{(2\pi c_\sigma^2)^{D/2}} \exp\left[-\frac{(c_\alpha - u_\alpha)^2}{2c_\sigma^2}\right], \tag{5}$$

where τ_σ is the relaxation time for self-collisions, $\tau_{\sigma\varsigma} = \tau_{\varsigma\sigma}\rho_\varsigma/\rho_\sigma$ is the relaxation time for cross collisions, $c_\sigma = \sqrt{k_B T/m_\sigma}$, k_B is the Boltzmann constant, and m_σ is the mass of a σ molecule. When $\beta=0$, the original model of Sirovich is recovered.

The discrete velocity Boltzmann (DVB) equation for the binary mixture [30] can be written as

$$\partial_t f_i^\sigma + c_{i\alpha,\sigma}\partial_\alpha f_i^\sigma = J_i^{\sigma\sigma} + J_i^{\sigma\varsigma} + F_i^\sigma, \tag{6}$$

where f_i^σ is the distribution function of the species σ for the discrete velocities $c_{i\alpha,\sigma}$. The linear collision operators and forcing terms are given by

$$J_i^{\sigma\sigma} = -\frac{1}{\tau_\sigma}(f_i^\sigma - f_i^{\sigma(0)}), \tag{7}$$

$$J_i^{\sigma\varsigma} = -\frac{1}{\tau_D}\frac{w_i\rho_\varsigma\rho_\sigma}{\rho}\frac{c_{i\alpha,\sigma}(u_\alpha^\sigma - u_\alpha^\varsigma)}{c_{s,\sigma}^2}, \tag{8}$$

$$f_i^{\sigma(0)} = w_i\rho_\sigma\left(1 + \frac{u_\alpha^\sigma c_{i\alpha,\sigma}}{c_\sigma^2}\right), \tag{9}$$

$$F_i^\sigma = w_i\frac{g_\alpha^\sigma c_{i\alpha,\sigma}}{c_\sigma^2}, \tag{10}$$

where τ_D is the relaxation time, and w_i is the weight for the discrete velocity $c_{i\alpha}$. In microscale flows with low Mach number, higher-order terms in the equilibrium functions and the forcing term have negligible influence on the evolution of conserved moments, and only the linear terms are retained here [31]. The form of the linear equilbrium functions does not depend on β. For the two-dimensional nine-velocity (D2Q9) scheme, the discrete velocities are given as

$$c_{ix,\sigma} = \sqrt{3}c_\sigma\{0,1,0,-1,0,1,-1,-1,1\}, \tag{11}$$

$$c_{iy,\sigma} = \sqrt{3}c_\sigma\{0,0,1,0,-1,1,1,-1,-1\}, \tag{12}$$

where $i=0,1,\ldots,8$. The weights are given as $w_0=4/9$, $w_1=w_2=w_3=w_4=1/9$, and $w_5=w_6=w_7=w_8=1/36$. The fourth-order Gauss-Hermite quadrature uses the quadrature points, $\pm a$ and $\pm b$, with the weights w_a and w_b, respectively, where $a=\sqrt{3-\sqrt{6}}$, $b=\sqrt{3+\sqrt{6}}$, $w_a=(3+\sqrt{6})/12$, and $w_b=(3-\sqrt{6})/12$. The two-dimensional (2D) quadrature D2Q16 can be obtained by the product formula of the 1D fourth-order Gauss-Hermite quadrature [32,23]. Here, the discrete velocities are indexed as

$$c_{ix,\sigma} = c_\sigma\{a,-a,b,-b,a,-a,b,-b,a,-a,b,-b,a,-a,b,-b\}, \tag{13}$$

$$c_{iy,\sigma} = c_\sigma\{a,a,a,a,-a,-a,-a,-a,b,b,b,b,-b,-b,-b,-b\}, \tag{14}$$

where $i=1,2,\ldots,16$.

The species density ρ_σ and the species momentum density j_α^σ are the lower moments of the distribution functions:

$$\sum f_i^\sigma = \rho_\sigma, \tag{15}$$

$$\sum c_{i\alpha,\alpha} f_i^\sigma = j_\alpha^\sigma = \rho_\sigma u_\alpha^\sigma. \tag{16}$$

The fluid mixture density ρ and barycentric velocity u_α are given by

$$\rho = \rho_\sigma + \rho_\varsigma, \tag{17}$$

$$j_\alpha = \rho u_\alpha = \rho_\sigma u_\alpha^\sigma + \rho_\varsigma u_\alpha^\varsigma. \tag{18}$$

The dynamic viscosity for the DVB equation is given by

$$\nu = p(X_\sigma\tau_\sigma + X_\varsigma\tau_\varsigma), \tag{19}$$

where p is the pressure and X_j is the mole fraction of species j. In multicomponent mixtures, however, the viscosity is not the linear function given in Eq. (19) but shows complex dependence on X_j. To remedy this deficiency of the BGK model, the viscosity is assumed to be given by the modified Wilke formula [33,34]:

$$\nu = \sum_j \frac{X_j\nu_j}{\Sigma_k X_k \Phi_{jk}}, \tag{20}$$

where

$$\Phi_{jk} = \frac{1}{\sqrt{8}}\left(1 + \frac{m_j}{m_k}\right)^{-1/2}\left[1 + \left(\frac{\nu_j}{\nu_k}\right)^{1/2}\left(\frac{m_k}{m_j}\right)^{1/4}\right]^2.$$

The relaxation time τ_j is then given by [25]

$$\tau_j = \frac{\nu_j}{p\Sigma_k X_k \Phi_{jk}}. \tag{21}$$

The relaxation time τ_D is determined by the binary diffusion coefficient D.

B. Finite difference lattice Boltzmann equation

In the multispeed LB methods for multicomponent mixtures, because of the variations in the speed of sound due to

different species masses, not all of the quadrature points coincide with the lattice points. Therefore the propagation-collision dynamics are not applicable. While several approaches have been proposed to apply the LB method in the off-lattice grid system, the finite difference method [35,36] is employed here.

Applying the forward Euler method for time discretization and the second-order total variation diminishing (TVD) scheme for spatial discretization, we obtain

$$\begin{aligned} f_i^\sigma(x,y,t+\delta t) = f_i^\sigma(x,y,t) + \Omega_i^\sigma(x,y,t)\,\delta t + F_i^\sigma(x,y,t)\,\delta t \\ + \delta t \frac{|c_{ix,\sigma}|}{\delta x}\left[f_i^\sigma\left(x + \frac{c_{ix,\sigma}}{|c_{ix,\sigma}|}\frac{\delta x}{2}, y, t\right)\right. \\ \left. - f_i^\sigma\left(x - \frac{c_{ix,\sigma}}{|c_{ix,\sigma}|}\frac{\delta x}{2}, y, t\right)\right] \\ + \delta t \frac{|c_{iy,\sigma}|}{\delta x}\left[f_i^\sigma\left(x, y + \frac{c_{iy,\sigma}}{|c_{iy,\sigma}|}\frac{\delta x}{2}, t\right)\right. \\ \left. - f_i^\sigma\left(x, y - \frac{c_{iy,\sigma}}{|c_{iy,\sigma}|}\frac{\delta x}{2}, t\right)\right], \end{aligned} \tag{22}$$

where δt and δx are the time step and the (uniform) grid spacing, respectively. The face values are given by

$$\begin{aligned} f_i^\sigma\left(x + \frac{c_{ix,\sigma}}{|c_{ix,\sigma}|}\frac{\delta x}{2}, y, t\right) = f_i^\sigma(x,y,t) \\ + \frac{\psi}{2}\left[f_i^\sigma\left(x + \frac{c_{ix,\sigma}}{|c_{ix,\sigma}|}\delta x, y, t\right)\right. \\ \left. - f_i^\sigma(x,y,t)\right]. \end{aligned} \tag{23}$$

The flux limiter ψ is chosen such that the scheme is globally of second order and TVD. The MUSCL scheme of van Leer [37] is used here for the flux limiter. While the implicit treatment of the collision terms improves the numerical stability in high Reynolds number (Re) flows [36], it is not essential for low Re flows.

III. MOLECULAR AND KNUDSEN DIFFUSION IN NARROW CHANNELS

The analytic solution of the DVB equation for the binary mixture is obtained for the problem of diffusion in narrow channels. Since the LB equation is consistent with the DVB equation when $\delta t \to 0$ and $\delta x \to 0$, the DVB equation will also be referred to as the LB equation, hereafter, for convenience. The solution method is based on that of Ansumali *et al.* [22], where a moment system corresponding to the LB equation is solved.

The species diffusion is driven by a constant concentration gradient in the opposite direction for the two species. The pressure gradient is therefore zero. The fluid particles are assumed to be reflected diffusely on a wall. This simple problem contains the essential features of multicomponent diffusion at finite Kn. The distribution of the species mass flux along the transverse direction y and the total species mass flux are obtained and compared with DSMC solutions for a range of Kn defined by λ/H, where λ and H are the mean free path of the molecules and the channel height, respectively. Impermeable walls are located at $y=H/2$ and $-H/2$.

In multicomponent mixtures, the mean free path can be defined by

$$\lambda = \sum_j X_j \lambda_j, \tag{24}$$

where λ_j is the mean free path of the (single component) species j for given p and T, and given by [21]

$$\lambda_j = \sqrt{\frac{\pi}{2}}\frac{\nu_j c_j}{p}. \tag{25}$$

From these equations, the dynamic viscosities ν_σ and ν_ς for given p and T are obtained, and the relaxation times τ_σ and τ_ς are determined by Eq. (21). Considering that the mean free path is not well defined except for hard-sphere molecules [21], an alternative definition of the mean free path [9,26] can also be used. For meaningful comparisons, however, the definition of the mean free path used in the LB method should be consistent with that in other reference methods [21]. Here, the definition of Eq. (24) is used for both the LB method and the DSMC method.

A. Standard LB method

For the standard D2Q9 scheme, a moment system m_j^σ can be written as [22,38]

$$m_j^\sigma = \sum_i e_{j,i}^\sigma f_i^\sigma = \{\rho^\sigma, j_x^\sigma, j_y^\sigma, P_{xx}^\sigma, P_{xy}^\sigma, P_{yy}^\sigma, Q_{xyy}^\sigma, Q_{yxx}^\sigma, R^\sigma\}, \tag{26}$$

where

$$\begin{aligned} e_{j,i}^\sigma = \{1, c_{ix,\sigma}, c_{iy,\sigma}, c_{ix,\sigma}^2, c_{ix,\sigma}c_{iy,\sigma}, c_{iy,\sigma}^2, c_{ix,\sigma}c_{iy,\sigma}^2, c_{iy,\sigma}c_{ix,\sigma}^2, \\ (c_{ix,\sigma}^2 - c_\sigma^2)(c_{iy,\sigma}^2 - c_\sigma^2)\}. \end{aligned} \tag{27}$$

Equations for all moments m_j^σ can be derived from the LB equation. Here, we will only derive an analytic expression for mass fluxes.

For the present problem, we replace the concentration gradient with a body force $\rho_\sigma h_\sigma$ and use the decomposition $c_\sigma^2\rho_{\sigma,0} = c_\sigma^2\rho_\sigma + \rho_\sigma h_\sigma x$, where x is the streamwise direction. Then, $j_y^\sigma = 0$ and ρ_σ is spatially uniform. The species mass flux is obtained from the following equations:

$$\partial_y P_{xy}^\sigma = \rho_\sigma h_\sigma - \frac{1}{\tau_D} j_x^{\sigma\varsigma}, \tag{28}$$

$$\partial_y Q_{xyy}^\sigma = -\frac{1}{\tau} P_{xy}^\sigma, \tag{29}$$

$$3c_\sigma^2 \partial_y P_{xy}^\sigma = -\frac{1}{\tau}(Q_{xyy}^\sigma - c_\sigma^2 \rho_\sigma u_x^\sigma) - \frac{c_\sigma^2}{\tau_D} j_x^{\sigma\varsigma} + c_\sigma^2 \rho_\sigma h_\sigma, \tag{30}$$

where $j_x^{\sigma\varsigma} = \rho_\sigma\rho_\varsigma/\rho(u_x^\sigma - u_x^\varsigma)$. From Eqs. (28) and (30), the energy flux Q_{xyy}^σ is given by

$$Q_{xyy}^{\sigma} = -2\tau c_{\sigma}^2\left(\rho_{\sigma}h_{\sigma} - \frac{1}{\tau_D}j_x^{\sigma\varsigma}\right) + c_{\sigma}^2\rho_{\sigma}u_x^{\sigma}. \tag{31}$$

Substituting this equation into Eq. (29) and differentiating the resulting equation with respect to y, we obtain

$$\rho_{\sigma}\partial_y^2 u_x^{\sigma} = -2\frac{\tau_{\sigma}}{\tau_D}\partial_y^2 j_x^{\sigma\varsigma} - \frac{1}{\tau_{\sigma}c_{\sigma}^2\tau_D}(\tau_D\rho_{\sigma}h_{\sigma} - j_x^{\sigma\varsigma}), \tag{32}$$

from which we obtain

$$(\eta + 2\mu_1)\partial_y^2 j_x^{\sigma\varsigma} = -\frac{1}{\tau^2 c_s^2\mu_2}[\tau_D\rho_{\sigma}h_{\sigma} - j_x^{\sigma\varsigma}], \tag{33}$$

$$\partial_y^2 j_x = -2\frac{\mu_{m1}}{\eta}\partial_y^2 j_x^{\sigma\varsigma} - \frac{\mu_{m2}}{\tau^2 c_s^2\eta}[\tau_D\rho_{\sigma}h_{\sigma} - j_x^{\sigma\varsigma}], \tag{34}$$

where $\tau = \sqrt{\tau_{\sigma}\tau_{\varsigma}}$, $\mu_{\sigma} = \tau_{\sigma}/\tau$, $\eta = \tau_D/\tau$, $\mu_{m1} = \mu_{\sigma} - \mu_{\varsigma}$, $\mu_1 = (X_{\varsigma}m_{\varsigma}\mu_{\sigma} + X_{\sigma}m_{\sigma}\mu_{\varsigma})/m$, $\mu_2 = m/[\sqrt{m_{\sigma}m_{\varsigma}}(\mu_{\sigma}X_{\sigma} + \mu_{\varsigma}X_{\varsigma})]$, $m = m_{\sigma}X_{\sigma} + m_{\varsigma}X_{\varsigma}$, $\mu_{m2} = (\mu_{\varsigma}m_{\sigma} - \mu_{\sigma}m_{\varsigma})/\sqrt{m_{\sigma}m_{\zeta}}$, and $c_s = \sqrt{c_{\sigma}c_{\varsigma}}$. X_{σ} is the mole fraction of species σ.

For a system without a wall, the left-hand side of Eq. (33) vanishes, and the diffusion flux is given by the classical Fick's law of diffusion:

$$j_x^{\sigma\zeta} = \tau_D\rho_{\sigma}h_{\sigma} = -\rho D\nabla Y_{\sigma}, \tag{35}$$

where Y_{σ} is the mass fraction of species σ. In general, the solution can be written as

$$\bar{j}_x^{\sigma\varsigma} = A\cosh\left(\lambda\frac{y}{\tau c_s}\right), \tag{36}$$

$$j_x = \left(-2\frac{\mu_{m1}}{\eta} + \frac{\mu_{m2}}{\lambda^2\eta}\right)\bar{j}_x^{\sigma\varsigma} + B, \tag{37}$$

where

$$\bar{j}_x^{\sigma\varsigma} = j_x^{\sigma\varsigma} - \tau_D\rho_{\sigma}h_{\sigma}, \tag{38}$$

$$\lambda = \frac{1}{\sqrt{(2\mu_1 + \eta)\mu_2}}. \tag{39}$$

The shear stress is given by

$$P_{xy}^{\sigma} = -\frac{Ac_s}{\lambda\eta}\sinh\left(\lambda\frac{y}{\tau c_s}\right). \tag{40}$$

When obtaining Eqs. (36) and (40), the symmetry condition is used.

The constant A can be obtained from the boundary condition of the distribution functions. At the bottom wall, the particles are reflected diffusely. The kinetic boundary condition with diffuse scattering kernel [17] can be written as

$$f_i^{\sigma}|_{y=-H/2} = \Psi f_i^{\sigma(0)}|_w, \quad \text{for } c_{iy,\sigma} > 0, \tag{41}$$

where

$$\Psi = \frac{\Sigma_{(c_{j\alpha,\sigma} - u_{\alpha w})n_{\alpha} < 0}|(c_{j\alpha,\sigma} - u_{\alpha w})n_{\alpha}|\, f_j^{\sigma}|_{y=-H/2}}{\Sigma_{(c_{k\alpha,\sigma} - u_{\alpha w})n_{\alpha} < 0}|(c_{k\alpha,\sigma} - u_{\alpha w})n_{\alpha}|\, f_k^{\sigma(0)}|_w}. \tag{42}$$

Here, n_{α} is the inward wall-normal vector, $u_{\alpha w}$ is the velocity of the wall, and $f_i^{\sigma(\mathrm{eq})}|_w$ is the equilibrium distribution evaluated using wall boundary conditions. For the present problem, the diffuse scattering boundary condition reduces to [31]

$$f_i^{\sigma}|_{y=-H/2} = f_i^{\sigma(0)}|_w = \rho_{\sigma}w_i, \quad \text{for } c_{iy} > 0. \tag{43}$$

The nonequilibrium distribution function at the wall is then given by

$$f_i^{\sigma(\mathrm{neq})}|_{y=-H/2} = \rho_{\sigma}w_i - f_i^{\sigma(0)}|_{y=-H/2}, \quad \text{for } c_{iy} > 0. \tag{44}$$

Using Eq. (44), we obtain

$$\left[\frac{c_{\sigma}}{\rho_{\sigma}}(f_5^{\sigma(\mathrm{neq})} - f_6^{\sigma(\mathrm{neq})}) - \frac{c_{\varsigma}}{\rho_{\varsigma}}(f_5^{\varsigma(\mathrm{neq})} - f_6^{\varsigma(\mathrm{neq})})\right]_{y=-H/2} = -\frac{\sqrt{3}}{18}u_x^{\sigma\varsigma}|_{y=-H/2} = -\frac{\sqrt{3}}{18}\frac{\rho}{\rho_{\varsigma}\rho_{\sigma}}[\tau_D\rho_{\sigma}h_{\sigma} + A\cosh(\lambda\alpha/2)], \tag{45}$$

where $\alpha = H/(\tau c_s)$. Alternatively, the nonequilibrium distribution function can be obtained using the linear relationship between the distribution functions and the moments:

$$\begin{aligned} f_i^{\sigma(\mathrm{neq})} = w_i\Bigg[&\frac{P_{xx}^{\sigma(\mathrm{neq})}}{2c_{\sigma}^4}(c_{ix,\sigma}^2 - c_{\sigma}^2) + \frac{P_{xy}^{\sigma(\mathrm{neq})}}{c_{\sigma}^4}c_{ix,\sigma}c_{iy,\sigma} \\ &+ \frac{P_{yy}^{\sigma(\mathrm{neq})}}{2c_{\sigma}^4}(c_{iy,\sigma}^2 - c_{\sigma}^2) + \frac{Q_{xyy}^{\sigma(\mathrm{neq})}}{2c_{\sigma}^6}c_{ix,\sigma}(c_{iy,\sigma}^2 - c_{\sigma}^2) \\ &+ \frac{Q_{yxx}^{\sigma(\mathrm{neq})}}{2c_{\sigma}^6}c_{iy,\sigma}(c_{ix,\sigma}^2 - c_{\sigma}^2) + \frac{R^{\sigma(\mathrm{neq})}}{2c_{\sigma}^8}(c_{ix,\sigma}^2 - c_{\sigma}^2) \\ &\times(c_{iy,\sigma}^2 - c_{\sigma}^2)\Bigg], \end{aligned} \tag{46}$$

where the superscript, neq, represents the nonequilibrium part of the quantity. Evaluating Eq. (46) at the bottom wall gives

$$\begin{aligned} &\left[\frac{c_{\sigma}}{\rho_{\sigma}}(f_5^{\sigma(\mathrm{neq})} - f_6^{\sigma(\mathrm{neq})}) - \frac{c_{\varsigma}}{\rho_{\varsigma}}(f_5^{\varsigma(\mathrm{neq})} - f_6^{\varsigma(\mathrm{neq})})\right]_{y=-H/2} \\ &= \frac{c_{\sigma}}{\rho_{\sigma}}\left[\frac{P_{xy}^{\sigma(\mathrm{neq})}}{6c_{\sigma}^2} + \frac{\sqrt{3}}{18}\frac{Q_{xyy}^{\sigma(\mathrm{neq})}}{c_{\sigma}^3}\right]_{y=-H/2} - \frac{c_{\varsigma}}{\rho_{\varsigma}}\left[\frac{P_{xy}^{\varsigma(\mathrm{neq})}}{6c_{\varsigma}^2}\right. \\ &\left. + \frac{\sqrt{3}}{18}\frac{Q_{xyy}^{\varsigma(\mathrm{neq})}}{c_{\varsigma}^3}\right]_{y=-H/2} = \frac{\rho}{\rho_{\varsigma}\rho_{\sigma}}\frac{A\mu_3}{6\lambda\eta}\sinh(\lambda\alpha/2) \\ &+ \frac{\rho}{\rho_{\varsigma}\rho_{\sigma}}\frac{\sqrt{3}\mu_1}{9}\frac{A}{\eta}\cosh(\lambda\alpha/2), \end{aligned} \tag{47}$$

where $\mu_3 = (\rho_{\sigma}c_{\sigma} + \rho_{\varsigma}c_{\varsigma})/(\rho c_s) = (m_{\sigma}^{3/4}m_{\varsigma}^{1/4}X_{\sigma} + m_{\varsigma}^{3/4}m_{\sigma}^{1/4}X_{\varsigma})/m$. Comparing Eqs. (45) and (47), we obtain

$$A = -\frac{\tau_D \rho_\sigma h_\sigma}{(1+2\mu_1/\eta)\cosh(\lambda\alpha/2) + \sqrt{3}\mu_3/(\lambda\eta)\sinh(\lambda\alpha/2)}. \tag{48}$$

Similarly, the coefficient B can be determined as

$$B = \tau_D \rho_\sigma h_\sigma \frac{\mu_{m2}/\lambda^2 + \sqrt{3}\mu_{m3}/\lambda \tanh(\lambda\alpha/2)}{\eta + 2\mu_1 + \sqrt{3}\mu_3/\lambda \tanh(\lambda\alpha/2)}, \tag{49}$$

where $\mu_{m3}=(\sqrt{m_\sigma}-\sqrt{m_\varsigma})/(m_\sigma m_\varsigma)^{1/4}$. The diffusion flux and the total mass flux are, respectively, given by

$$\hat{j}_x^{\sigma\varsigma} = 1 - \frac{\phi(\alpha\hat{y};\lambda)}{(1+2\mu_1/\eta)\phi(\alpha/2;\lambda) + \sqrt{3}\mu_2/(\lambda\eta)\psi(\alpha/2;\lambda)}, \tag{50}$$

$$\hat{j}_x = \left(-2\frac{\mu_{m1}}{\eta} + \frac{\mu_{m2}}{\lambda^2\eta}\right)(\hat{j}_x^{\sigma\varsigma} - 1) + \frac{\mu_{m2}/\lambda^2 + \sqrt{3}\mu_{m3}/\lambda \tanh(\lambda\alpha/2)}{\eta + 2\mu_1 + \sqrt{3}\mu_3/\lambda \tanh(\lambda\alpha/2)}, \tag{51}$$

where $\hat{j}_x^{\sigma\varsigma}=j_x^{\sigma\varsigma}/(\tau_D\rho_\sigma h_\sigma)$, $\hat{j}_x=j_x/(\tau_D\rho_\sigma h_\sigma)$, $\hat{y}=y/H$ and $\phi(\alpha\hat{y};\lambda)=\cosh(\lambda\alpha\hat{y})\exp(-\lambda\alpha/2)$ and $\psi(\alpha\hat{y};\lambda)=\sinh(\lambda\alpha\hat{y})\exp(-\lambda\alpha/2)$. Integrating along the channel and normalizing, we obtain

$$Q^{\sigma\varsigma} = 1 - \frac{2}{\lambda\alpha}\frac{\psi(\alpha/2;\lambda)}{(1+2\mu_1/\eta)\phi(\alpha/2;\lambda) + \sqrt{3}/(\lambda\eta)\psi(\alpha/2;\lambda)}, \tag{52}$$

$$Q = \left(-2\frac{\mu_{m1}}{\eta} + \frac{\mu_{m2}}{\lambda^2\eta}\right)(Q^{\sigma\varsigma} - 1) + \frac{\mu_{m2}/\lambda^2 + \sqrt{3}\mu_{m3}/\lambda \tanh(\lambda\alpha/2)}{\eta + 2\mu_1 + \sqrt{3}\mu_3/\lambda \tanh(\lambda\alpha/2)}, \tag{53}$$

where

$$Q^{\sigma\varsigma} = \int_{-1/2}^{1/2} \hat{j}_x^{\sigma\varsigma} d\hat{y},$$

$$Q = \int_{-1/2}^{1/2} \hat{j}_x d\hat{y}.$$

B. Higher-order LB method

The moment system for D2Q16 [38] can be written as

$$m_j^\sigma = \sum_i e_{j,i}^\sigma f_i^\sigma = \{\rho^\sigma, j_x^\sigma, j_y^\sigma, P_{xx}^\sigma, P_{xy}^\sigma, P_{yy}^\sigma, Q_{xyy}^\sigma, Q_{yxx}^\sigma, Q_{xxx}^\sigma, Q_{yyy}^\sigma, R_x^\sigma, R_y^\sigma, R^\sigma, S_x^\sigma, S_y^\sigma, S^\sigma\}, \tag{54}$$

where

$$e_{j,i}^\sigma = \{1, c_{ix,\sigma}, c_{iy,\sigma}, c_{ix,\sigma}^2, c_{ix,\sigma}c_{iy,\sigma}, c_{iy,\sigma}^2, c_{ix,\sigma}c_{iy,\sigma}^2, c_{iy,\sigma}c_{ix,\sigma}^2, c_{ix,\sigma}^3, c_{iy,\sigma}^3, (c_{ix,\sigma}^2 - 3c_\sigma^2)c_{ix,\sigma}c_{iy,\sigma}, (c_{iy,\sigma}^2 - 3c_\sigma^2)c_{ix,\sigma}c_{iy,\sigma}, (c_{ix,\sigma}^2 - c_\sigma^2) \times (c_{iy,\sigma}^2 - c_\sigma^2), c_{ix,\sigma}(c_{ix,\sigma}^2 - 3c_\sigma^2)(c_{iy,\sigma}^2 - 3c_\sigma^2), c_{iy,\sigma}(c_{ix,\sigma}^2 - 3c_\sigma^2)(c_{iy,\sigma}^2 - 3c_\sigma^2), c_{ix,\sigma}c_{iy,\sigma}(c_{ix,\sigma}^2 - 3c_\sigma^2)(c_{iy,\sigma}^2 - 3c_\sigma^2)\}. \tag{55}$$

For D2Q16, the species mass flux can be obtained by solving the following moment equations:

$$\partial_y P_{xy}^\sigma = \rho_\sigma h_\sigma - \frac{1}{\tau_D} j_x^{\sigma\varsigma}, \tag{56}$$

$$\partial_y Q_{xyy}^\sigma = -\frac{1}{\tau_\sigma} P_{xy}^\sigma, \tag{57}$$

$$\partial_y (R_y^\sigma + 3c_\sigma^2 P_{xy}^\sigma) = -\frac{1}{\tau_\sigma}(Q_{xyy}^\sigma - c_\sigma^2 \rho_\sigma u_x^\sigma) + c_\sigma^2\left(\rho_\sigma h_\sigma - \frac{1}{\tau_D} j_x^{\sigma\varsigma}\right), \tag{58}$$

$$\partial_y (3c_\sigma^2 Q_{xyy}^\sigma - 3c_\sigma^4 \rho_\sigma u_x^\sigma) = -\frac{1}{\tau_\sigma} R_y^\sigma. \tag{59}$$

From these equations we obtain

$$\mu_4 \bar{j}_x^{\sigma\varsigma} - (5\mu_5 + \eta\mu_6)\tau^2 c_s^2 \partial_y^2 \bar{j}_x^{\sigma\varsigma} + 3\mu_7 \eta\tau^4 c_s^4 \partial_y^4 j_x^{\sigma\varsigma} = \frac{\mu_1(X_\sigma - X_\varsigma)}{2}\eta\tau^2 c_s^2 \partial_y^2 j_x - 3\frac{\mu_{m8}}{2}\eta\tau^4 c_s^4 \partial_y^4 j_x, \tag{60}$$

$$\mu_{m4} \bar{j}_x^{\sigma\varsigma} - (5\mu_{m5} + \eta\mu_{m6})\tau^2 c_s^2 \partial_y^2 \bar{j}_x^{\sigma\varsigma} + 3\mu_{m7} \eta\tau^4 c_s^4 \partial_y^4 j_x^{\sigma\varsigma} = \frac{\mu_1}{2}\eta\tau^2 c_s^2 \partial_y^2 j_x - 3\frac{\mu_8}{2}\eta\tau^4 c_s^4 \partial_y^4 j_x, \tag{61}$$

where $\mu_4=(\mu_\sigma+\mu_\varsigma)/2$, $\mu_{4m}=(\mu_\sigma-\mu_\varsigma)/2$, $\mu_5=(\mu_\sigma\sqrt{m_\varsigma/m_\sigma} + \mu_\varsigma\sqrt{m_\sigma/m_\varsigma})/2$, $\mu_{m5}=(\mu_\sigma\sqrt{m_\varsigma/m_\sigma}-\mu_\varsigma\sqrt{m_\sigma/m_\varsigma})/2$, $\mu_6=(\sqrt{m_\varsigma/m_\sigma}+\sqrt{m_\sigma/m_\varsigma})/2$, $\mu_{m6}=(\sqrt{m_\varsigma/m_\sigma}-\sqrt{m_\sigma/m_\varsigma})/2$, $\mu_7=(\mu_\sigma^2 m_\varsigma/m_\sigma+\mu_\varsigma^2 m_\sigma/m_\varsigma)/2$, $\mu_{m7}=(\mu_\sigma^2 m_\varsigma/m_\sigma-\mu_\varsigma^2 m_\sigma/m_\varsigma)/2$, $\mu_8=(\mu_\sigma m_\varsigma X_\sigma+\mu_\varsigma m_\sigma X_\varsigma)/(2m)$, and $\mu_{m8}=(\mu_\sigma m_\varsigma X_\sigma - \mu_\varsigma m_\sigma X_\varsigma)/(2m)$. The solution of these equations is very complex and, here, we only obtain the solution for the special case where $m_\sigma=m_\varsigma$.

When $m_\sigma=m_\varsigma$, the equation for $j_x^{\sigma\varsigma}$ reduces to

$$\bar{j}_x^{\sigma s} - (5+\eta)\tau^2 c_s^2 \partial_y^2 \bar{j}_x^{\sigma s} + 3\eta\tau^4 c_s^4 \partial_y^4 j_x^{\sigma s} = 0. \quad (62)$$

The solution for $\hat{j}_x^{\sigma s}$ can be written as

$$\hat{j}_x^{\sigma s} = 1 + \hat{A}_{16}\phi(\alpha\hat{y};\lambda_1) + \hat{B}_{16}\phi(\alpha\hat{y};\lambda_2), \quad (63)$$

where

$$\lambda_1 = \sqrt{\frac{5+\eta+\sqrt{(\eta+5)^2-12\eta}}{6\eta}}, \quad (64)$$

$$\lambda_2 = \sqrt{\frac{5+\eta-\sqrt{(\eta+5)^2-12\eta}}{6\eta}}. \quad (65)$$

Similar to the procedure outlined for D2Q9 above, the integration constants, $\hat{A}$ and $\hat{B}$, can be obtained from the boundary condition of the distribution functions:

$$\hat{A}_{16} = -\frac{B_b - B_a}{B_b A_a - B_a A_b}, \quad (66)$$

$$\hat{B}_{16} = -\frac{A_b - A_a}{A_b B_a - A_a B_b}, \quad (67)$$

where

$$A_a = \left[1 + \frac{(a^2-1)}{2}\left(\frac{1}{\eta\lambda_1^2} - 1\right)\right]\phi(\alpha/2;\lambda_1) + \left[\frac{1}{\eta\lambda_1} - \frac{\sqrt{6}}{2}\left(\frac{1}{\eta\lambda_1} - \lambda_1\right)\right]a\psi(\alpha/2;\lambda_1), \quad (68)$$

$$A_b = \left[1 + \frac{(b^2-1)}{2}\left(\frac{1}{\eta\lambda_1^2} - 1\right)\right]\phi(\alpha/2;\lambda_1) + \left[\frac{1}{\eta\lambda_1} + \frac{\sqrt{6}}{2}\left(\frac{1}{\eta\lambda_1} - \lambda_1\right)\right]b\psi(\alpha/2;\lambda_1), \quad (69)$$

$$B_a = \left[1 + \frac{(a^2-1)}{2}\left(\frac{1}{\eta\lambda_2^2} - 1\right)\right]\phi(\alpha/2;\lambda_2) + \left[\frac{1}{\eta\lambda_2} - \frac{\sqrt{6}}{2}\left(\frac{1}{\eta\lambda_2} - \lambda_1\right)\right]a\psi(\alpha/2;\lambda_2), \quad (70)$$

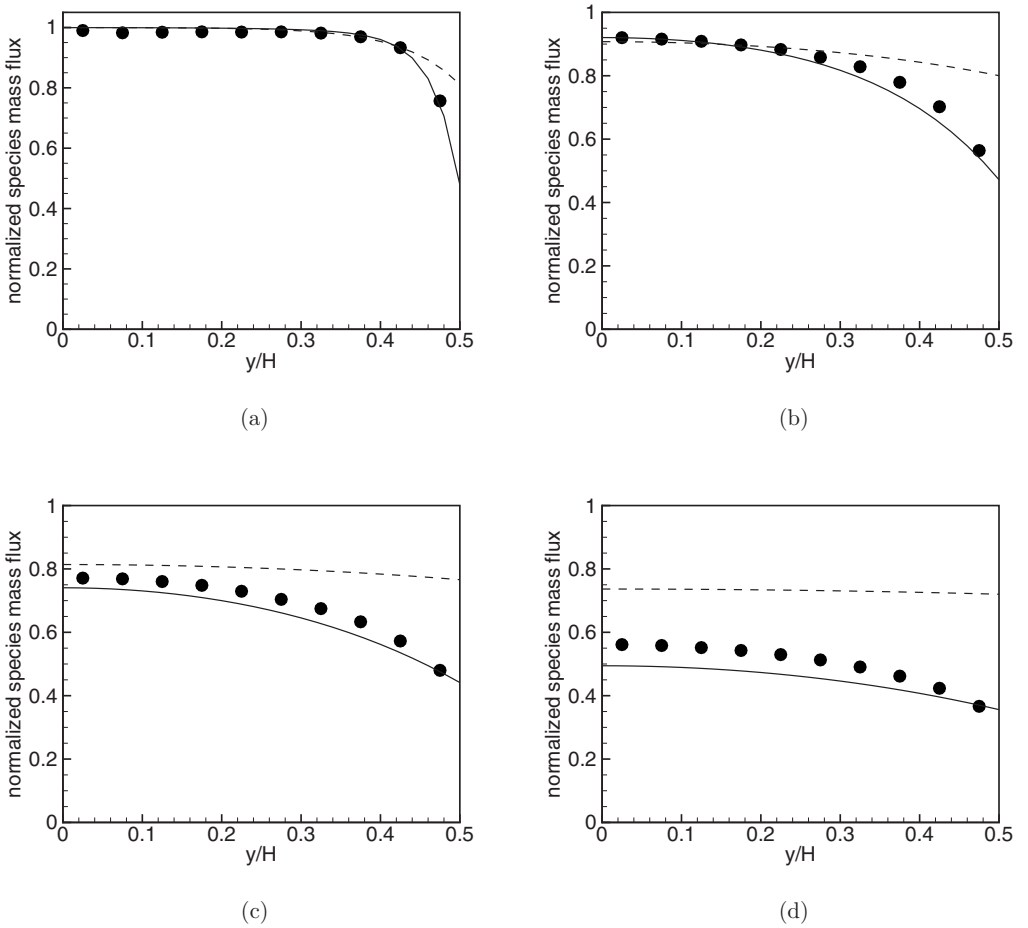

FIG. 1. Distribution of the normalized species mass flux across the channel for $m_s/m_\sigma = 1$. (a) Kn=0.05, (b) Kn=0.25, (c) Kn=0.5, and (d) Kn=1 (symbols: DSMC; solid lines: D2Q16; dashed lines: D2Q9).

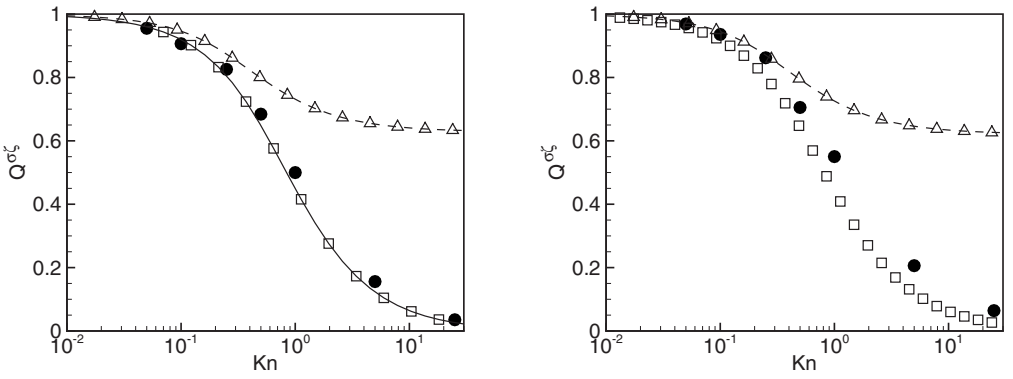

FIG. 2. Normalized total species mass flow rate as a function of Kn. (a) $m_s/m_\sigma=1$ and (b) $m_s/m_\sigma=2$ (symbols: DSMC; solid lines: D2Q16; squares: D2Q16 numerical simulations; dashed lines: D2Q9; triangles: D2Q9 numerical simulations; $X_\sigma=0.5$).

$$B_b = \left[1 + \frac{(b^2-1)}{2}\left(\frac{1}{\eta\lambda_2^2} - 1\right)\right]\phi(\alpha/2;\lambda_2) + \left[\frac{1}{\eta\lambda_2} + \frac{\sqrt{6}}{2}\left(\frac{1}{\eta\lambda_2} - \lambda_2\right)\right] b\psi(\alpha/2;\lambda_2). \quad (71)$$

The algebraic transformation specific to D2Q16 can be found in [31], where analytic solutions for single-component Poiseuille flows are obtained. The total species mass flow rate is given by

$$Q^{\sigma s} = 1 + \frac{2\hat{A}}{\lambda_1\alpha}\psi(\alpha/2;\lambda_1) + \frac{2\hat{B}}{\lambda_2\alpha}\psi(\alpha/2;\lambda_2). \quad (72)$$

IV. RESULTS AND DISCUSSION

The analytic and numerical solutions for the LB methods are compared with results from the DSMC method. In the DSMC simulations, hard-sphere molecules are used, and the collision cross sections [26] are identical for all collision types. For the higher-order LB method, only numerical solutions are presented, when species masses in the mixture are different. For the numerical simulations, the transverse direction is discretized into 50 lattices.

A. Diffusional flux

Figure 1 shows the distribution of the species mass flux normalized by $-\rho D\nabla Y^\sigma$, for $m_s/m_\sigma=1$. As discussed above, the normalized species mass flux $\hat{j}_x^\sigma$ is unity when the mixture is not confined. Note the kinetic layer near the wall boundary in Fig. 1. At small Knudsen number, Kn=0.05, $\hat{j}_x^\sigma$ is close to unity at $y/H<0.35$, and the species mass flux obeys Fick's law of diffusion. At $y/H>0.35$, the normalized species mass flux rapidly decreases toward the wall. While D2Q9 captures the exponential decay of the species mass flux in the kinetic layer, it gives higher species mass flux than the DSMC method near the wall. The higher-order scheme D2Q16 is in excellent agreement with the DSMC method. As Kn increases, the effects of walls become more important, and even near the centerline $\hat{j}_x^\sigma$ is reduced to about 0.92 for Kn=0.25. For Kn=0.5 and 1.0, the shape of $\hat{j}_x^\sigma$ is similar to that for Kn=0.25. However, $\hat{j}_x^\sigma$ at the same y rapidly decreases as Kn increases.

In the present study, fluid particles are assumed to be diffusely reflected on walls. For small Kn, the fluid mixture outside the kinetic layer is very close to equilibrium and the normalized species mass flux is close to unity. The nonequilibrium terms are significant only in the kinetic layer, the thickness of which is of the order of the mean free path, and vanish exponentially toward the center of the channel. Because of the rapid change of the equilibrium distribution in the kinetic layer, the nonequilibrium effects are much more significant than those in single-component Poiseuille flows. This results in the large slip velocity of individual species even for small Kn. When $\mathrm{Kn}\ll 1$ and $m_\sigma=m_s$, the normalized species mass flux at a wall is given by $(2\lambda+\sqrt{3})/(\lambda\eta+2\lambda+\sqrt{3})$ for D2Q9. For a ratio of relaxation times $\eta=1.2$, which is the value used in Figs. 1 and 2(a), the component slip is about 0.81, which is significantly higher than the values obtained in DSMC and D2Q16 for Kn=0.05. For this case, the component slip in D2Q16 is about 0.5 when $\mathrm{Kn}\ll 1$.

Figure 2 shows the normalized mass flow rate $Q^{\sigma s}$ for $m_s/m_\sigma=1$ and 2, as a function of Kn. For very small Kn, the diffusion flux is governed by Fick's law of diffusion in most of the channel, and $Q^{\sigma s}$ is close to unity. The mass flow rate $Q^{\sigma s}$ decreases with Kn, because collisions with walls inhibit diffusion fluxes. For very large Kn, diffusion processes are governed only by collisions with walls, and the diffusion flux is given by

$$j_x^{\sigma s} = -\rho D_K \nabla Y^\sigma, \quad (73)$$

where D_K is the Knudsen diffusivity. The Knudsen diffusivity scales as

$$D_K \sim c_s H. \quad (74)$$

Therefore, as $\mathrm{Kn}\to\infty$, using the definition of $Q^{\sigma s}$ and the relation $\lambda\sim\tau_D c_s$, the normalized mass flow rate can be approximated as

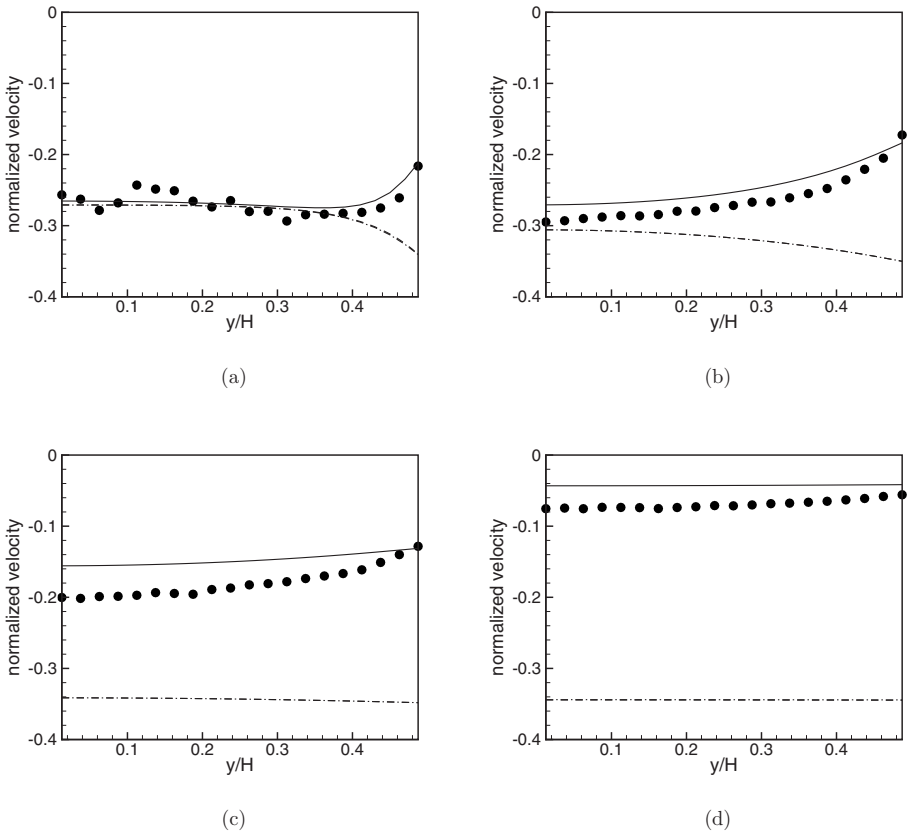

FIG. 3. Normalized velocity for $m_s/m_\sigma=2$ and $X_\sigma=0.5$. (a) Kn=0.05, (b) Kn=0.25, (c) Kn=1, and (d) Kn=5 (symbols: DSMC; solid lines: D2Q16 numerical simulations; dashed lines: D2Q9; dashed dotted lines: D2Q9 numerical simulations).

$$Q^{\sigma s} \sim \frac{1}{\mathrm{Kn}}. \tag{75}$$

For Kn=$O(10)$, however, the analysis of the data shows that the mass flow rate $Q^{\sigma s}$ decreases more slowly than in Eq. (75) due to the small but finite number of molecular collisions. The asymptotic limit for large Kn is well reproduced by DSMC and D2Q16, while D2Q9 fails in the Knudsen diffusion regime. As Kn$\to\infty$, the mass flow rate $Q^{\sigma s}$ for D2Q9 approaches $2\mu_1/(2\mu_1+\eta)$. The higher-order scheme D2Q16 is in good agreement with DSMC for Kn=$O(0.1)$, while it slightly underpredicts the mass flow rate for large Kn numbers.

B. Diffusion slip

Figure 3 shows the normalized velocity, $\hat{u}_x(=\hat{j}_x/\hat{\rho})$, for $m_s/m_\sigma=2$ and $X_\sigma=0.5$ at various Kn numbers. The analytic

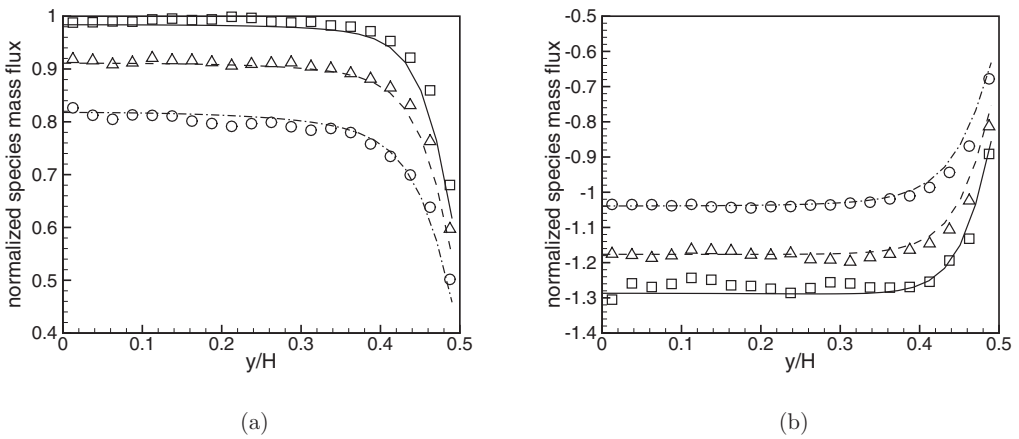

FIG. 4. Normalized species mass flux for different mole fractions. (a) $\hat{j}_x^\sigma$ (b) $\hat{j}_x^s$ (squares: DSMC for $X_\sigma=0.1$, triangles: DSMC for $X_\sigma=0.5$, circles: DSMC for $X_\sigma=0.9$, solid lines: D2Q16 for $X_\sigma=0.1$, dashed lines: D2Q16 for $X_\sigma=0.5$, dashed lines: D2Q16 for $X_\sigma=0.9$; $m_s/m_\sigma=2$; Kn=0.05).

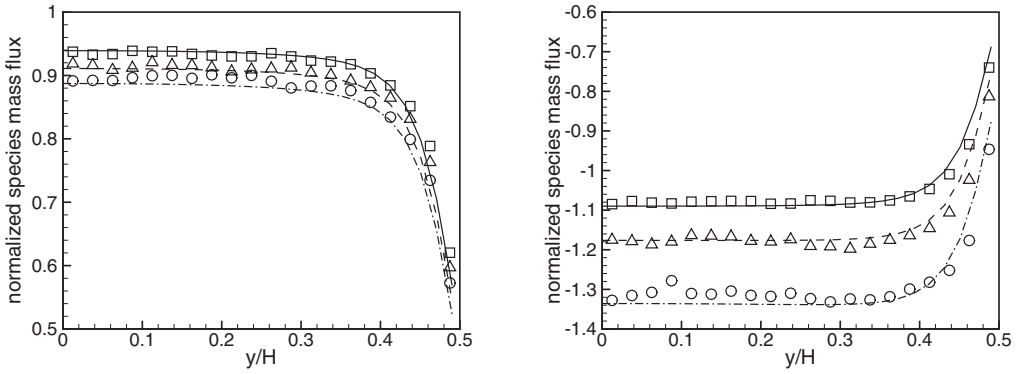

(a) (b)

FIG. 5. Normalized species mass flux for different mass ratio m_s/m_σ. (a) $\hat{j}_x^\sigma$ (b) $\hat{j}_x^s$ (squares: DSMC for $m_s/m_\sigma=1.5$; triangles: DSMC for $m_s/m_\sigma=2$; circles: DSMC for $m_s/m_\sigma=3$; solid lines: D2Q16 for $m_s/m_\sigma=1.5$; dashed lines: D2Q16 for $m_s/m_\sigma=2$; dashed lines: D2Q16 for $m_s/m_\sigma=3$; $X_\sigma=0.5$; Kn=0.05).

solutions for D2Q9 are almost identical to the numerical solutions. For Kn=0.05, both D2Q9 and D2Q16 performs well near the centerline. However, D2Q9 fails in the Knudsen layer. Note that D2Q9 does not correctly describe the decrease of the diffusion slip velocity with Kn. For very high Kn numbers, $\hat{u}_x$ for D2Q9 is given by

$$\hat{u}_x = 2\frac{\mu_{m1}}{\eta} + \mu_{m2}\left(\frac{1}{\lambda^2(\eta+2\mu_1)} - \frac{1}{\lambda^2\eta}\right). \tag{76}$$

D2Q16 well reproduces the characteristics observed in the DSMC simulations, and gives much better results than D2Q9 for all Kn numbers.

Figure 4 shows the normalized species mass flux for $X_\sigma=0.1$, 0.5, and 0.9 at Kn=0.05. The mass ratio m_s/m_σ is 2. The species mass fluxes, $\hat{j}_x^\sigma$ and $\hat{j}_x^s$, decrease in magnitude, as the mass fraction of the lighter species increases. D2Q16 well reproduces the characteristics observed in DSMC. Near the centerline, $\hat{j}_x^j$ approaches unity, as X_j approaches zero.

The normalized species mass flux for varying mass ratio is shown in Fig. 5. The higher-order LB method well reproduces the dependence of the species mass fluxes on the mass ratio m_σ/m_s in DSMC. The statistical error for DSMC becomes more significant as the mass of a heavier species increases.

In isobaric diffusion problems where the pressure is constant, the diffusion slip provides a theoretical explanation of Graham's law [39]:

$$-\frac{X_\sigma u_x^\sigma}{X_s u_x^s} = \sqrt{\frac{m_s}{m_\sigma}}. \tag{77}$$

Graham's law is an empirical relation and validated by several experimental data, especially for high mass ratio mixtures [39]. However, the molar flux ratios from the LB method and the DSMC method do not follow Graham's law for the present cases, although the discrepancy is not large. From Eq. (32), it can be shown that the standard LB method follows the Graham's law for all Kn and all locations only when $\mu_\sigma/\mu_s=\sqrt{m_\sigma/m_s}$. In Fig. 5, at the center of the channel, the molar flux ratio for the LB method with the Wilke formula follows

$$-\frac{X_\sigma u_x^\sigma}{X_s u_x^s} \approx \left(\frac{m_s}{m_\sigma}\right)^{0.4}. \tag{78}$$

This relation is also observed in the DSMC results.

Figure 6 shows the normalized total mass flow rate Q as a function of the mass ratio m_s/m_σ. The magnitude of the diffusion slip velocity increases with m_s/m_σ, and both D2Q16 and D2Q9 well reproduce the trend observed in DSMC. However, accurate description of the mixture viscosity using, for example, Wilke formula is required for quantitative prediction. With the original BGK formulation, where the relax-

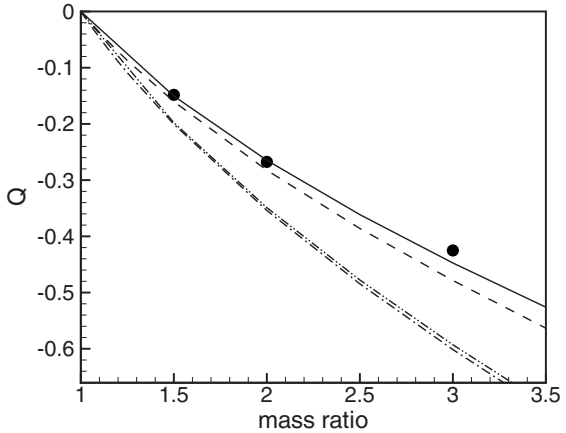

FIG. 6. Normalized total mass flow rate for different mass ratio m_s/m_σ at Kn=0.05 and $X_\sigma=0.5$ (circles: DSMC; solid line: D2Q16 with Wilke formula, dashed line: D2Q9 with Wilke formula; dashed dotted line: D2Q16 without Wilke formula; dashed double-dotted line: D2Q9 without Wilke formula).

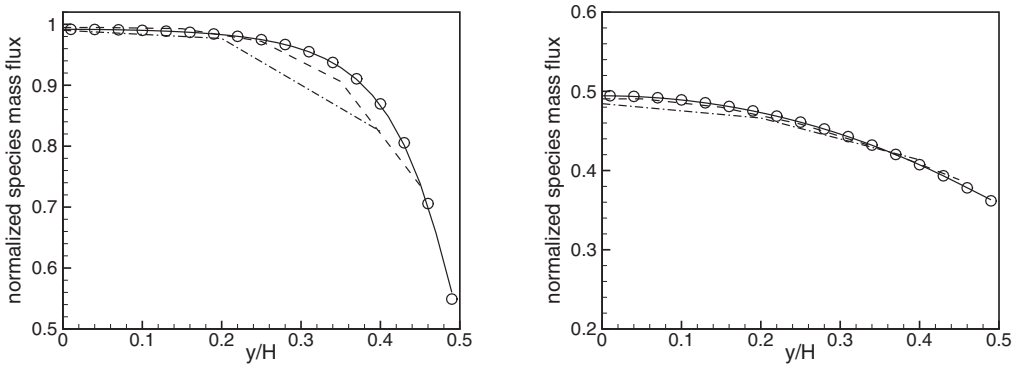

(a) (b)

FIG. 7. Comparison of numerical solutions for the diffusion flux for D2Q16 with the analytic solution. (a) Kn=0.1 and (b) Kn=1 (symbols: analytic solution; dashed dotted line: numerical solution with $N=5$; dashed line: numerical solution with $N=10$; solid line: numerical solution with $N=50$; $m_s/m_\sigma=1$).

ation time τ_j is given by $\tau_j=\nu_j/p$, the diffusion slip velocity is overpredicted in Fig. 6.

C. Discrete lattice effects

The analytic solutions are obtained for the DVB equation. Due to finite lattice spacing, the LB method involves discretization errors or discrete lattice effects [40]. The discrete lattice effects result not only from the discretization of the DVB equation itself but also from the boundary condition [21,41,42]. The discretization scheme used in the present finite difference LB method is of $O(\delta x^2)$. For the boundary closure, the halfway scheme is used to obtain second-order accuracy for a straight wall [18,19,43–45]. Here, fluid lattices in the transverse direction are indexed from 1 to N, while the boundary lattices are 0 and $N+1$. In the halfway scheme, the boundary lattices are located at $y=-H/2-\delta/2$ for the wall boundary located at $y=-H/2$, while the boundary lattices are located at $y=H/2+\delta/2$ for the upper wall. The unknown distribution functions at the wall boundary lattices are given by Eq. (43).

In Fig. 7, numerical solutions for various resolutions are compared with the analytic solution for D2Q16 at Kn=0.1 and 1.0. Even for low resolution of $N=5$, the kinetic layer is captured and the overall mass flow rate is well predicted. The numerical solution is in excellent agreement with the analytic solution for $N=50$.

Figure 8 shows the spatial discretization errors for the diffusion flux predicted by D2Q16 for a mixture of species with equal molecular masses. The error is defined by

$$\epsilon=\frac{|Q_a^{\sigma s}-Q_n^{\sigma s}|}{Q_a^{\sigma s}},$$

where $Q_a^{\sigma s}$ and $Q_n^{\sigma s}$ are the diffusion flux obtained from the analytic solutions and from the numerical simulations, respectively. For both Kn=0.1 and 1, the present scheme is approximately of second order except for the low resolution

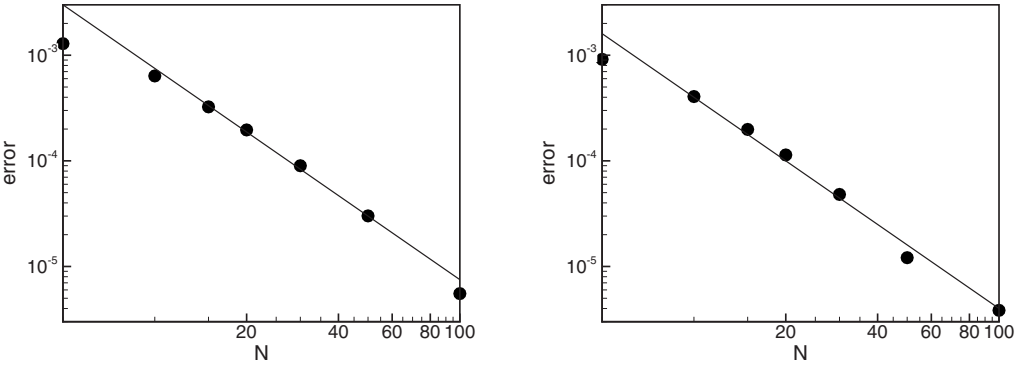

(a) (b)

FIG. 8. Errors due to the spatial discretization in the diffusion flux for (a) Kn=0.1 and (b) Kn=1 (symbols: D2Q16; solid lines: second-order accuracy; $m_s/m_\sigma=1$).

of $N \approx 5$. However, the errors are only about 0.1% even for this low resolution.

V. CONCLUSIONS

The lattice Boltzmann modeling of multicomponent diffusion for finite Knudsen numbers is investigated. Analytic solutions for binary diffusion in narrow channels, where both molecular and Knudsen diffusion are of importance, are obtained for the standard and higher-order LB methods and validated against the results from the direct simulation Monte Carlo method. For a higher-order LB method with the D2Q16 quadrature, the analytic solution is obtained only for the mixture consisting of equal-mass species.

The LB methods are shown to reproduce the diffusion slip phenomena. However, a modified formulation for the mixture viscosity is required for quantitative prediction, and the kinetic layer predicted by the standard LB method is qualitatively different from that in DSMC simulations. In addition, the standard LB method fails to predict the asymptotic behavior of the total mass flow rate and diffusion flux in the Knudsen diffusion regime. A higher-order LB method based on the fourth-order Gauss-Hermite quadrature captures the characteristics observed in the DSMC method with good accuracy. Graham's law is found to be invalid for the problems considered here, although the discrepancy is not large.

ACKNOWLEDGMENT

Financial support by Honda R&D Co., Ltd., Fundamental Technology Research Center, is gratefully acknowledged.

[1] A. Fick, Ann. Phys. **170**, 59 (1855).
[2] M. Knudsen, Ann. Phys. **333**, 75 (1909).
[3] J. Koplik and J. R. Banavar, Phys. Rev. Lett. **80**, 5125 (1998).
[4] H. Brenner and V. Ganesan, Phys. Rev. E **61**, 6879 (2000).
[5] C. Denniston and M. O. Robbins, Phys. Rev. Lett. **87**, 178302 (2001).
[6] G. Mo and F. Rosenberger, Phys. Rev. A **44**, 4978 (1991).
[7] I. N. Ivchenko and Y. I. Yalamov, Fluid Dyn. **6**, 570 (1971).
[8] S. Takata, S. Yasuda, S. Kosuge, and K. Aoki, Phys. Fluids **15**, 3745 (2003).
[9] F. Sharipov and D. Kalempa, Phys. Fluids **16**, 3779 (2004).
[10] H. A. Kramers and J. Kistemaker, Physica (Amsterdam) **10**, 699 (1943).
[11] G. R. McNamara and G. Zanetti, Phys. Rev. Lett. **61**, 2332 (1988).
[12] Y. H. Qian, D. d'Humières, and P. Lallemand, Europhys. Lett. **17**, 479 (1992).
[13] S. Chen and G. D. Doolen, Annu. Rev. Fluid Mech. **30**, 329 (1998).
[14] R. Benzi, S. Succi, and M. Vergassola, Phys. Rep. **222**, 145 (1992).
[15] S. Succi, *The Lattice Boltzmann Equation for Fluid Dynamics and Beyond* (Oxford University Press, Oxford, 2001).
[16] S. Succi, Phys. Rev. Lett. **89**, 064502 (2002).
[17] S. Ansumali and I. V. Karlin, Phys. Rev. E **66**, 026311 (2002).
[18] V. Sofonea and R. F. Sekerka, J. Comput. Phys. **207**, 639 (2005).
[19] M. Sbragaglia and S. Succi, Phys. Fluids **17**, 093602 (2005).
[20] R. Zhang, X. Shan, and H. Chen, Phys. Rev. E **74**, 046703 (2006).
[21] S. H. Kim, H. Pitsch, and I. D. Boyd, Phys. Rev. E **77**, 026704 (2008).
[22] S. Ansumali, I. V. Karlin, S. Arcidiacono, A. Abbas, and N. I. Prasianakis, Phys. Rev. Lett. **98**, 124502 (2007).
[23] X. Shan, X.-F. Yuan, and H. Chen, J. Fluid Mech. **550**, 413 (2006).
[24] S. H. Kim, H. Pitsch, and I. D. Boyd, J. Comput. Phys. **229**, 8655 (2008b).
[25] S. Arcidiacono, I. V. Karlin, J. Mantzaras, and C. E. Frouzakis, Phys. Rev. E **76**, 046703 (2007).
[26] G. A. Bird, *Molecular Gas Dynamics and the Direct Simulation of Gas Flows* (Oxford University Press, Oxford, 1994).
[27] E. P. Gross and K. M., Phys. Rev. **102**, 593 (1956).
[28] L. Sirovich, Phys. Fluids **5**, 908 (1962).
[29] P. Asinari and L.-S. Luo, J. Comput. Phys. **227**, 3878 (2008).
[30] L. S. Luo and S. S. Girimaji, Phys. Rev. E **67**, 036302 (2003).
[31] S. H. Kim and H. Pitsch, Phys. Rev. E **78**, 016702 (2008).
[32] S. Ansumali, I. V. Karlin, and H. C. Ottinger, Europhys. Lett. **63**, 798 (2003).
[33] C. R. Wilke, J. Chem. Phys. **18**, 517 (1950).
[34] R. B. Bird, W. B. Stewart, and E. N. Lightfoot, *Transport Phenomena* (Wiley and Sons, New York, 2002).
[35] R. Mei and W. Shyy, J. Comput. Phys. **143**, 426 (1998).
[36] Z. Guo and T. S. Zhao, Phys. Rev. E **67**, 066709 (2003).
[37] B. van Leer, J. Comput. Phys. **32**, 101 (1979).
[38] I. V. Karlin and S. Ansumali, Phys. Rev. E **76**, 025701(R) (2007).
[39] A. F. Mills, Physica A **371**, 256 (2006).
[40] Z. Guo, C. Zheng, and B. Shi, Phys. Rev. E **65**, 046308 (2002).
[41] Z. Guo, B. Shi, T. S. Zhao, and C. Zheng, Phys. Rev. E **76**, 056704 (2007).
[42] F. Verhaeghe, L.-S. Luo, and B. Blanpain, J. Comput. Phys. **228**, 147 (2009).
[43] R. Cornubert, D. d'Humières, and D. Levermore, Physica D **47**, 241 (1991).
[44] I. Ginzbourg and P. M. Adler, J. Phys. II **4**, 191 (1994).
[45] X. He, Q. Zou, L.-S. Luo, and M. Dembo, J. Stat. Phys. **87**, 115 (1997).